

# DATA-TO-ENERGY STOCHASTIC DYNAMICS

**Kirill Tamogashev**

University of Edinburgh  
k.tamogashev@sms.ed.ac.uk

**Nikolay Malkin**

University of Edinburgh, CIFAR Fellow  
nmalkin@ed.ac.uk

 [mmacosha/d2e-stochastic-dynamics](https://github.com/mmacosha/d2e-stochastic-dynamics)

## ABSTRACT

The Schrödinger bridge problem is concerned with finding a stochastic dynamical system bridging two marginal distributions that minimises a certain transportation cost. This problem, which represents a generalisation of optimal transport to the stochastic case, has received attention due to its connections to diffusion models and flow matching, as well as its applications in the natural sciences. However, all existing algorithms enable the inference of such dynamics only for cases where samples from both distributions are available. In this paper, we propose the first general method for modelling Schrödinger bridges when one (or both) distributions are given by their unnormalised densities, with no access to data samples. Our algorithm relies on a generalisation of the iterative proportional fitting (IPF) procedure to the data-free case, inspired by recent developments in off-policy reinforcement learning for training of diffusion samplers. We demonstrate the efficacy of the proposed *data-to-energy IPF* on synthetic problems, finding that it can successfully learn transports between multimodal distributions. As a secondary consequence of our reinforcement learning formulation, which assumes a fixed time discretisation scheme for the dynamics, we find that existing data-to-data Schrödinger bridge algorithms can be substantially improved by learning the diffusion coefficient of the dynamics. Finally, we apply the newly developed algorithm to the problem of sampling posterior distributions in latent spaces of generative models, thus creating a data-free image-to-image translation method.

## 1 INTRODUCTION

Two modern approaches to generative modelling that have paved the way for scalable and efficient generation of high-fidelity images (Dhariwal & Nichol, 2021; Rombach et al., 2021), videos (Polyak et al., 2024), audio (Chen et al., 2021a; Kong et al., 2021) and text (Nie et al., 2025; Sahoo et al., 2025) are diffusion models and flow matching. Diffusion models (Sohl-Dickstein et al., 2015; Ho et al., 2020; Song et al., 2021b) assume a noising stochastic process that transforms data into a tractable noise distribution and use score-based techniques to learn its reverse process, which transforms noise into data. Flow matching (Liu et al., 2023; Albergo et al., 2025; Lipman et al., 2023; Tong et al., 2024a) learns time-dependent deterministic dynamics that give a transportation map between two arbitrary distributions. Both approaches can be seen as special cases of the more general problem of learning stochastic dynamics between two arbitrary distributions.

The problem of inferring an optimal stochastic bridge between two distributions is called the Schrödinger bridge (SB) problem. Initially proposed in Schrödinger (1931; 1932), it has recently been studied using various machine learning techniques (Huang et al., 2021; Vargas et al., 2021; Chen et al., 2021b; Stromme, 2023; Shi et al., 2023; Tong et al., 2024b). One computational approach to the Schrödinger bridge problem is the iterative proportional fitting (IPF) algorithm (Fortet, 1940; Vargas et al., 2021; De Bortoli et al., 2021), which maintains a pair of processes in forward and reverse time and iteratively updates them by solving half-bridge problems (see §2). Upon convergence, the two processes become time reversals of each other and solve the SB problem. Notably, the typical training of diffusion models – with a fixed noising process that transforms a data distribution into a Gaussian by construction – is a degenerate case of IPF that converges in a single step. However, existing variants of IPF work only in a setting where samples from both marginal distributions are

available and thus cannot be used to model bridges when one (or both) of the marginal distributions is given as an unnormalised density, without access to data samples.

We propose to extend the IPF algorithm to the case where one or both marginal distributions are given by unnormalised densities or energy functions:  $p(x) = e^{-\mathcal{E}(x)}/Z$ ,  $Z = \int e^{-\mathcal{E}(x)} dx$ , where  $\mathcal{E}$  can be queried, but  $Z$  is unknown. Our proposed *data-to-energy* (or *energy-to-energy*) IPF generalises recently developed techniques for training diffusion models to sample from a distribution given by an unnormalised density (Zhang & Chen, 2022; Vargas et al., 2023; 2024; Berner et al., 2024; Albergo & Vanden-Eijnden, 2025; Blessing et al., 2025a, *inter alia*). In particular, we build upon off-policy reinforcement learning losses and stabilisation techniques for diffusion samplers (Richter et al., 2020; Richter & Berner, 2024; Lahlou et al., 2023; Sendera et al., 2024; Gritsaev et al., 2025) to propose an efficient training for the IPF steps in the data-to-energy setting. Our algorithm is the first general method for inferring data-to-energy and energy-to-energy Schrödinger bridges.

Wielding the newly proposed algorithm, we make three contributions:

- (1) We show that the proposed data-to-energy and energy-to-energy IPF algorithms successfully learn stochastic bridges with low transport cost between synthetic datasets and densities, performing on par with the transports learnt by data-to-data IPF using samples from a ground-truth oracle.
- (2) As a secondary contribution, we show that – as a consequence of the time discretisation used in our reinforcement learning formulation – existing data-to-data IPF algorithms can be improved by learning the diffusion coefficient of the dynamics, in addition to the drift, generalising the results of Gritsaev et al. (2025) for diffusion samplers to the more general SB setting.
- (3) We apply the data-to-energy IPF algorithm to the problem of translating prior distributions to posteriors in latent spaces of generative models, generalising the outsourced diffusion sampling of Venkatraman et al. (2025) to yield a scalable data-free image-to-image translation method.

## 2 DATA-TO-DATA SCHRÖDINGER BRIDGES

### 2.1 ITERATIVE PROPORTIONAL FITTING FOR DATA-TO-DATA SB

**Setting: The SB problem and its connection to optimal transport.** We present some background on the SB problem; see Léonard (2014); De Bortoli et al. (2021) for relevant and more detailed overviews. Let  $p_0$  and  $p_1$  be two given distributions over the space  $\mathbb{R}^d$ , assumed to be absolutely continuous (thus used interchangeably with their density functions) and of finite variance. Let  $\mathbb{Q}_t$  be a reference process on the time interval  $[0, 1]$  taking values in  $\mathbb{R}^d$  (usually an Ornstein-Uhlenbeck process, such as the Wiener process). The Schrödinger bridge problem can be formalised as:

$$\mathbb{P}_t^* = \underset{\mathbb{P}_t}{\operatorname{argmin}} \{ \operatorname{KL}(\mathbb{P}_t \parallel \mathbb{Q}_t) \text{ s.t. } (\pi_0)_\# \mathbb{P}_t = p_0, (\pi_1)_\# \mathbb{P}_t = p_1 \}, \quad (1)$$

where the minimisation is taken over all processes  $\mathbb{P}_t$  whose marginals at times  $t = 0$  and  $t = 1$ , written  $(\pi_0)_\# \mathbb{P}_t$  and  $(\pi_1)_\# \mathbb{P}_t$ , equal  $p_0$  and  $p_1$ , respectively. The solution  $\mathbb{P}_t^*$  is a stochastic dynamical system that transports  $p_0$  to  $p_1$  – that is, a *bridge* – that is the closest to  $\mathbb{Q}_t$  in KL divergence. If the reference process  $\mathbb{Q}_t$  is given by an Itô stochastic differential equation (SDE)

$$\mathbb{Q}_t : \quad dX_t = F_{\text{ref}}(X_t, t) dt + \sigma_t dW_t, \quad X_0 \sim q_0,$$

then, under mild conditions (see Léonard (2014)) the solution to (1) exists, is unique, and also takes the form of an SDE:

$$\mathbb{P}_t : \quad dX_t = F(X_t, t) dt + \sigma_t dW_t, \quad X_0 \sim p_0.$$

with the same diffusion coefficient. The KL then takes the form of a dynamic transport cost (Berner et al., 2026)

$$\operatorname{KL}(\mathbb{P}_t \parallel \mathbb{Q}_t) = \operatorname{KL}(p_0 \parallel q_0) + \mathbb{E}_{X_t \sim \mathbb{P}_t} \int_0^1 \frac{\|F_{\text{ref}}(X_t, t) - F(X_t, t)\|^2}{2\sigma_t^2} dt, \quad (2)$$

reducing the problem (1) to one of inferring the drift function  $F$  minimising the cost (2). This representation makes clear that as  $\sigma_t \rightarrow 0$ , the SB problem approaches the dynamic optimal transport problem between  $p_0$  and  $p_1$  with squared-euclidean cost (see Tong et al. (2024a)). For  $\sigma_t > 0$ , the joint marginal distribution of  $\mathbb{P}_t^*$  over  $X_0, X_1$  is an *entropy-regularised* optimal transport, a key observation in the derivation of the SB algorithm in Tong et al. (2024b).

**Iterative proportional fitting.** Computationally, the SB problem can be solved using the iterative proportional fitting (IPF) algorithm (Fortet, 1940; Vargas et al., 2021; De Bortoli et al., 2021). IPF defines a recursion initialised at  $\vec{\mathbb{P}}_t^0 = \mathbb{Q}_t$ :

$$\vec{\mathbb{P}}_t^{n+1} = \operatorname{argmin}_{\mathbb{P}_t} \left\{ \text{KL}(\mathbb{P}_t \parallel \vec{\mathbb{P}}_t^n) \text{ s.t. } (\pi_0)_{\#} \mathbb{P}_t = p_0 \right\} = p_0 \otimes \vec{\mathbb{P}}_{t|0}^n, \quad (3a)$$

$$\overleftarrow{\mathbb{P}}_t^{n+1} = \operatorname{argmin}_{\mathbb{P}_t} \left\{ \text{KL}(\mathbb{P}_t \parallel \overleftarrow{\mathbb{P}}_t^{n+1}) \text{ s.t. } (\pi_1)_{\#} \mathbb{P}_t = p_1 \right\} = p_1 \otimes \overleftarrow{\mathbb{P}}_{t|1}^{n+1}, \quad (3b)$$

where each step is the solution to a *half-bridge* problem, which pins the previous iterate at one of the marginals  $p_0$  or  $p_1$  (here  $\vec{\mathbb{P}}_{t|0}^n$  denotes the conditional process given  $X_0$  and  $\overleftarrow{\mathbb{P}}_{t|1}^{n+1}$  the conditional process given  $X_1$ ). IPF for Schrödinger bridges is thus a dynamic generalisation of the Sinkhorn algorithm (Sinkhorn, 1964), which computes entropic optimal transport by iteratively renormalising a cost matrix over rows and columns. It can be shown (De Bortoli et al., 2021) that the iterates  $\vec{\mathbb{P}}_t^n$  and  $\overleftarrow{\mathbb{P}}_t^n$  converge to the same stochastic process and that this process solves the SB problem (1).

If  $\vec{\mathbb{P}}_t^0 = \mathbb{Q}_t$  is represented as an SDE, then the iterates defined in (3b) and (3a) can be represented as forward-time and reverse-time SDEs initialised at  $p_0$  and  $p_1$ , respectively. We can thus introduce SDEs with neurally parametrised drifts (Tzen & Raginsky, 2019):

$$\vec{\mathbb{P}}_t^n : d\vec{X}_t = \vec{F}_{\theta_n}(X_t, t) dt + \sigma_t d\vec{W}_t, \quad (4a)$$

$$\overleftarrow{\mathbb{P}}_t^n : d\overleftarrow{X}_t = \overleftarrow{F}_{\varphi_n}(X_t, t) dt + \sigma_t d\overleftarrow{W}_t, \quad (4b)$$

where  $\sigma_t$  coincides with the diffusion coefficient of the reference process, and perform the iterations (3) as optimisation problems over  $\theta_n$  and  $\varphi_n$ . (We henceforth occasionally drop the subscript  $n$  from the parameters, with the understanding that (3a) optimises  $\varphi = \varphi_{n+1}$  under a fixed  $\theta_n$  and (3b) optimises  $\theta = \theta_{n+1}$  under a fixed  $\varphi_{n+1}$ .)

**Data-to-data IPF in a time discretisation.** To approximately perform the optimisations involved in IPF with respect to the parameters  $\theta$  and  $\varphi$ , we discretise the SDEs (4) representing  $\vec{\mathbb{P}}_t$  and  $\overleftarrow{\mathbb{P}}_t$  over  $K$  steps using the Euler-Maruyama scheme with  $\Delta t = \frac{1}{K}$ . The continuous-time processes are thus approximated by discrete-time Markov chains, *i.e.*, joint distributions over discrete-time trajectories  $\tau = (x_0, x_{\Delta t}, \dots, x_1)$ , having the factorisation:

$$\vec{p}_{\theta}(\tau) = p_0(x_0) \prod_{k=0}^{K-1} \overbrace{\vec{p}_{\theta}(x_{(k+1)\Delta t} | x_{k\Delta t})}^{\vec{p}_{\theta}(\tau | x_0)}, \quad \overbrace{\vec{p}_{\theta}(x_{(k+1)\Delta t} | x_{k\Delta t}) = \mathcal{N}(x_{k\Delta t} + \vec{F}_{\theta}(x_{k\Delta t}, k\Delta t)\Delta t, \sigma_{k\Delta t}^2 \Delta t)}^{\text{Euler-Maruyama step with step size } \Delta t}, \quad (5a)$$

$$\overleftarrow{p}_{\varphi}(\tau) = p_1(x_1) \prod_{k=1}^K \overbrace{\overleftarrow{p}_{\varphi}(x_{(k-1)\Delta t} | x_{k\Delta t})}^{\overleftarrow{p}_{\varphi}(\tau | x_1)}, \quad \overbrace{\overleftarrow{p}_{\varphi}(x_{(k-1)\Delta t} | x_{k\Delta t}) = \mathcal{N}(x_{k\Delta t} + \overleftarrow{F}_{\varphi}(x_{k\Delta t}, k\Delta t)\Delta t, \sigma_{k\Delta t}^2 \Delta t)}^{\text{reverse-time Euler-Maruyama step with step size } \Delta t}. \quad (5b)$$

As proposed in Vargas et al. (2021), the two IPF optimisation problems in (3) can be approximately solved by maximum likelihood. On the level of the discretised processes, this amounts to the following recurrence:

$$\varphi_{n+1} = \operatorname{argmax}_{\varphi} \mathbb{E}_{x_0 \sim p_0, \tau \sim \vec{p}_{\theta_n}(\tau | x_0)} \sum_{k=1}^K \log \overleftarrow{p}_{\varphi}(x_{(k-1)\Delta t} | x_{k\Delta t}) \quad (6a)$$

$$\theta_{n+1} = \operatorname{argmax}_{\theta} \mathbb{E}_{x_1 \sim p_1, \tau \sim \overleftarrow{p}_{\varphi_{n+1}}(\tau | x_1)} \sum_{k=0}^{K-1} \log \vec{p}_{\theta}(x_{(k+1)\Delta t} | x_{k\Delta t}). \quad (6b)$$

The optimisation problem in (6a) (resp. (6b)) requires taking a sample from the marginal distribution  $x_0 \sim p_0$  (resp.  $x_1 \sim p_1$ ), rolling out a trajectory in forward time from  $\vec{p}_{\theta}$  (resp. in reverse time from  $\overleftarrow{p}_{\varphi}$ ) initialised at the sample, and maximising the log-likelihood of this trajectory in the opposite direction, *i.e.*, under  $\overleftarrow{p}_{\varphi}$  (resp. under  $\vec{p}_{\theta}$ ). This procedure essentially requires samples from  $p_0$  (resp. from  $p_1$ ) to be available.

Algorithm 1: Data-to-Data IPF	Algorithm 2: Data-to-Energy IPF
<pre> 1 <b>for</b> <math>n = 0, \dots, n_{\max}</math> <b>do</b>   /* Backward IPF step (6a) */ 2   <b>while not converged do</b> 3     <math>x_0 \sim p_0</math> 4     <math>\tau = (x_0, x_{\Delta t}, \dots, x_1) \sim \vec{p}_\theta(\tau   x_0)</math>       using (5a) 5     Gradient step on <math>\varphi</math> with       <math>\nabla \log \overleftarrow{p}_\varphi(\tau   x_1)</math>   /* Forward IPF step (6b) */ 6   <b>while not converged do</b> 7     <math>x_1 \sim p_1</math> 8     <math>\tau = (x_0, \dots, x_{1-\Delta t}, x_1) \sim \overleftarrow{p}_\varphi(\tau   x_1)</math>       using (5b) 9     Gradient step on <math>\theta</math> with       <math>\nabla \log \vec{p}_\theta(\tau   x_0)</math> 10 <b>return</b> <math>\theta, \varphi</math> </pre>	<pre> 1 <b>Initialise</b> buffer <math>\mathcal{B} = \emptyset</math> 2 <b>for</b> <math>n = 0, \dots, n_{\max}</math> <b>do</b>   /* Backward IPF step (6a) */ 3   <b>while not converged do</b> 4     <math>x_0 \sim p_0, \tau \sim \vec{p}_\theta(\tau   x_0)</math> 5     Gradient step on <math>\varphi</math> with       <math>\nabla \log \overleftarrow{p}_\varphi(\tau   x_1)</math> 6     <b>Update</b> <math>\mathcal{B}</math> with samples <math>x_1</math>   /* Forward IPF step (8) */ 7   <b>while not converged do</b> 8     <b>if on-policy then</b> 9       <math>x_0 \sim p_0, \tau \sim \vec{p}_\theta(\tau   x_0)</math> 10    <b>else</b> 11      <math>x_1 \sim \mathcal{B}, \tau^{(1)} \sim \overleftarrow{p}_\varphi(\tau   x_1)</math> 12      <math>\tau^{(2)}, \dots, \tau^{(N)} \sim \vec{p}_\theta(\tau   x_0^{(1)})</math> 13      Gradient step on <math>\theta</math> with       <math>\nabla \text{Var}_i \left( \log \frac{\vec{p}_\theta(\tau^{(i)}   x_0^{(1)})}{\overleftarrow{p}_\varphi(\tau^{(i)}   x_1^{(i)})} + \mathcal{E}_1(x_1^{(i)}) \right)</math> 14 <b>return</b> <math>\theta, \varphi</math> </pre>

Figure 1: **Left:** Algorithm for data-to-data IPF. **Right:** Algorithm for data-to-energy IPF, showing the replay buffer with backward trajectory reuse (§3.1), with differences highlighted in red.

We call this iterative algorithm the *log-likelihood method* and give an algorithmic presentation in Algorithm 1. It contrasts with the method proposed in De Bortoli et al. (2021), which uses a slightly different discretisation scheme, although the two coincide in the continuous-time limit ( $K \rightarrow \infty$ ).

**Diffusion models as a special case.** Diffusion models (Sohl-Dickstein et al., 2015; Ho et al., 2020; Song et al., 2021b) can be seen as a special case of the IPF algorithm that converges in a single step. If  $p_0$  is a data distribution and  $p_1$  is Gaussian, and  $\mathbb{Q}_t$  is a noising process that transports any source distribution to  $p_1$  by construction, then  $\mathbb{Q}_t$  initialised at  $p_0$  is already a bridge between  $p_0$  and  $p_1$ . Thus the first iteration of IPF – learning  $\overleftarrow{\mathbb{P}}_t^1$  by maximum-likelihood training (6a) on trajectories sampled from  $p_0 \otimes \mathbb{Q}_t |_0$  – already yields a bridge between  $p_0$  and  $p_1$ , so all subsequent iterations are redundant and  $\overleftarrow{\mathbb{P}}_t^1$  solves the SB problem. In practice, training  $\overleftarrow{\mathbb{P}}_t^1$  as a neural SDE proceeds by score matching, which is simply a Rao-Blackwellised estimate of the IPF maximum-likelihood objective (Song et al., 2021a).

## 2.2 DISCRETISATION ALLOWS FLEXIBLE KERNELS

The majority of existing work (Chen et al., 2021b; Vargas et al., 2021; De Bortoli et al., 2021; Shi et al., 2023) trains only the drift functions  $\vec{F}_\theta, \overleftarrow{F}_\varphi$  or related objects using objectives similar to (6). In contrast to that, **we propose to train not only the drift, but also diffusion coefficients of both processes**, by replacing the variances  $\sigma_{k\Delta t}^2$  in (5) by learnt functions  $\vec{\sigma}_\theta^2(x_k, k\Delta t)$  and  $\overleftarrow{\sigma}_\varphi^2(x_k, k\Delta t)$ . We expect this to correct for the effect of time discretisation error, inspired by the results for diffusion samplers in Gritsaev et al. (2025).

The optimisation problems in (6) can then be solved with respect to the parameters of both the drift and diffusion coefficients. We compare this approach to those that do not learn the variance in Table 1.

### 3 DATA-FREE SCHRÖDINGER BRIDGES

#### 3.1 IPF FOR DATA-TO-ENERGY SB

We now consider the setting where samples from  $p_0$  are available, but  $p_1$  is given by an unnormalised density  $p_1(x) = e^{-\mathcal{E}_1(x)}/Z$  and  $Z = \int e^{-\mathcal{E}_1(x)} dx$  is unknown. In this case, the odd-numbered IPF steps (3a) can be performed (via (6a)), but the even-numbered steps (3b) cannot be done using (6b), as they require samples from  $p_1$ . Instead, we need an objective that would fit  $\overrightarrow{\mathbb{P}}_t^{n+1}$  as a forward-time SDE matching  $p_1 \otimes \overleftarrow{\mathbb{P}}_{t|1}^{n+1}$  without samples from  $p_1$ .

In the time discretisation (5), the IPF step (3b) for  $\overrightarrow{\mathbb{P}}_t^{n+1}$  requires enforcing that for every  $x_0$ ,  $\overrightarrow{p}_\theta(\tau | x_0) \propto \overleftarrow{p}_\varphi(\tau | x_1)p_1(x_1)$  over all trajectories  $\tau = (x_0, x_{\Delta t}, \dots, x_1)$  starting at  $x_0$ .

To approximately enforce this proportionality, we introduce a source-conditional variant of the second-moment, or log-variance, loss used for training diffusion samplers (Richter et al. (2020); see Berner et al. (2026) for an overview of related losses and their consistency properties in the continuous-time limit). The idea is to minimise the variance of the log-ratio of the two sides of the proportionality over trajectories  $\tau$  sharing the same  $x_0$ :

$$\mathcal{L}_{LV}(x_0, \theta) = \text{Var} \left( \log \frac{\overrightarrow{p}_\theta(\tau | x_0)}{p_1(x_1) \overleftarrow{p}_\varphi(\tau | x_1)} \right) = \text{Var} \left( \sum_{k=1}^K \log \frac{\overrightarrow{p}_\theta(x_{k\Delta t} | x_{(k-1)\Delta t})}{\overleftarrow{p}_\varphi(x_{(k-1)\Delta t} | x_{k\Delta t})} + \mathcal{E}_1(x_1) \right), \quad (7)$$

where the variance is taken over some full-support distribution  $p^{\text{train}}(\cdot | x_0)$  over trajectories. (The normalising constant  $Z$  does not affect the variance, nor do we need to know the marginal of the process being learnt at time 0.) The empirical variance over a batch of  $N$  trajectories sampled from  $p^{\text{train}}(\tau | x_0)$  is an unbiased estimate of (7) and can be used in the loss. (The training policy we use below takes  $N$  *non-i.i.d.* trajectories, thus  $p^{\text{train}}(\cdot | x_0)$  can be a distribution over *batches* of  $\tau$ .)

Because this proportionality must hold for every  $x_0$ , we must also average (7) over  $x_0 \sim p_0^{\text{train}}(x_0)$ , where  $p_0^{\text{train}}$  is some training distribution over  $x_0$ . Thus the full objective for the forward IPF step is

$$\mathcal{L}(\theta) = \mathbb{E}_{x_0 \sim p_0^{\text{train}}(x_0)} \mathbb{E}_{\tau^{(1)}, \dots, \tau^{(N)} \sim p^{\text{train}}(\cdot | x_0)} \left[ \text{Var}_i \left( \log \frac{\overrightarrow{p}_\theta(\tau^{(i)} | x_0)}{\overleftarrow{p}_\varphi(\tau^{(i)} | x_1^{(i)})} + \mathcal{E}_1(x_1^{(i)}) \right) \right]. \quad (8)$$

The choice of  $p_0^{\text{train}}(x_0)$  and  $p^{\text{train}}(\cdot | x_0)$  is very important and we discuss it in the next subsection.

**Comparison with diffusion samplers.** The objective (7) is a conditional variant of the log-variance, or *VarGrad*, loss (Richter et al., 2020) previously used for diffusion-based samplers of unnormalised target densities. In that setting – *but not in ours*, since the marginal of  $p_1 \otimes \overleftarrow{\mathbb{P}}_{t|1}^{n+1}$  at time 0 is not  $p_0$  unless IPF has converged – the density of the process being learnt at time 0 is known to be  $p_0(x_0)$ . Thus  $p_0(x_0)$  can be placed in the numerator of the loss in (7) and variance can be taken over both  $x_0$  and  $\tau$ . An alternative objective would fit the density at  $x_0$ , yielding a variant of the related *trajectory balance* (TB) loss for diffusion samplers (Malkin et al., 2022; Lahlou et al., 2023).

Yet another alternative would avoid IPF altogether and simply perform joint optimisation of both  $\theta$  and  $\varphi$  using a VarGrad- or TB-like objective to enforce that  $p_0(x_0) \overrightarrow{p}_\theta(\tau | x_0) = p_1(x_1) \overleftarrow{p}_\varphi(\tau | x_1)$  over all trajectories  $\tau$ . Such a *bridge sampling* approach is taken in Blessing et al. (2025a;b); Gritsaev et al. (2025). However, this approach would yield a bridge that is not necessarily the solution to the SB problem (1), since the KL to the reference process is not minimised. In a future work, it would be interesting to compare our IPF approach with those that regularise bridge sampling losses by the cost (2).

#### 3.2 OFF-POLICY TRAINING METHODS

The objective (8) leaves room for the choice of training distributions  $p_0^{\text{train}}(x_0)$  and  $p^{\text{train}}(\tau | x_0)$ , which can vary over the course of training. In this way, training with this loss is a form of off-policy reinforcement learning, a connection that has been elucidated and exploited for improved training of diffusion samplers in Sendera et al. (2024).

A naïve choice would take  $p_0^{\text{train}} = p_0$  and  $p^{\text{train}}(\tau | x_0) = \overrightarrow{p}_\theta(\tau | x_0)$  (*on-policy* training). However, for complex, high-dimensional distributions on-policy training is insufficient, as modes that are not

discovered by the sampler are very unlikely to be explored. To facilitate training we adapt practices from diffusion sampling literature to guide the sampling process towards the areas of high density of the target distribution  $p_1$ . In the following paragraphs, we discuss such techniques.

**Replay buffer.** We keep a replay buffer of final samples  $x_1$  from the process  $\vec{p}_\theta(\tau | x_0)$ . During training, to obtain  $x_0$ , we sample  $x_1$  from the buffer, then sample a reverse trajectory to obtain  $x_0$  for training:  $\tilde{x}_0 \sim \overleftarrow{p}_\varphi(\cdot | x_1)$ . As the model trains and begins to better approximate  $p_1$ , the buffer becomes populated with samples  $x_1$  that are probable under  $p_1$ . Thus, the buffer helps the sampler focus on the relevant regions of the space and retain information about previously discovered modes.

**Reverse trajectories.** To obtain the batch of trajectories  $\tau$  starting at  $x_0$ , we use both the reverse trajectory used to produce  $x_0$  (see above) and a batch of  $N - 1$  trajectories drawn on-policy from  $\vec{p}_\theta(\tau | x_0)$  to form a batch of  $N$  trajectories sharing their initial point. The reuse of the backward trajectories allows the algorithm to learn on trajectories that reach high-density regions of  $p_1$ . However, using *only* reverse trajectories prevents the model from sufficiently exploring the whole space. Therefore, careful tuning is needed to strike a perfect balance between exploration and exploitation. We use  $N = 2$  for all our experiments.

**Langevin updates.** Following the method of Sendera et al. (2024) for diffusion samplers, we periodically update the buffer using a few steps of unadjusted Langevin on the density  $p_1$  to correct for the sampler’s imperfect fit to the target.

**Mixing on-policy and off-policy training.** In the training policy, we use a mixture of initial points  $x_0$  and trajectories  $\tau$  sampled on-policy and those sampled using the Langevin-updated buffer with reverse trajectory reuse, as described above. The frequency of using the buffer is called the *off-policy ratio*, and we ablate different off-policy ratios in Table 3. For most of the experiments we use constant off-policy ratio 0.8.

We provide details of all off-policy methods in Appendix D, and these methods are ablated in §5.4.

### 3.3 ITERATIVE PROPORTIONAL FITTING WITH DATA-TO-ENERGY STEPS

The full IPF algorithm for data-to-energy SB alternates between backward steps that train  $\varphi$  to convergence using the maximum-likelihood objective (6a) and forward steps that train  $\theta$  to convergence using (8). The backward step is trained using samples from  $p_0$  and forward trajectories from  $\vec{p}_\theta(\tau | x_0)$ , while the forward step is trained using trajectories obtained using the off-policy methods described above. The complete algorithm is summarised in Algorithm 2. We reuse the model weights and preserve the buffer state from the previous IPF step, although we randomly reinitialise a fraction of samples stored in buffer for the outsourced experiments.

**Energy-to-energy generalisation.** The data-to-energy IPF algorithm can easily be generalised to the case where samples from neither  $p_0$  nor  $p_1$  are available, but both are given by unnormalised densities  $p_i(x) = e^{-\mathcal{E}_i(x)}/Z_i$ . In this case, both the backward and forward IPF steps must be performed using the variance-based loss (7), with appropriate choices of training distributions (such as keeping separate replay buffers for both marginals). We call this *energy-to-energy* SB and show preliminary results in §5.2.

**Evaluation metrics.** We consider three metrics for evaluating the approximate solutions to the SB problem yielded by our data-to-energy IPF algorithm. Because SB is a constrained optimisation problem, it is necessary to measure both the constraint satisfaction (*i.e.*, that the solution is a transport from  $p_0$  to  $p_1$ ) and the cost (divergence from the reference process). To this end we measure ELBO, path KL, and Wasserstein distance to oracle samples from the target distribution (when available); see Appendix B for details.

## 4 OUTSOURCED SAMPLING WITH SCHRÖDINGER BRIDGES

We describe how our algorithm for solving data-to-energy Schrödinger bridges can be applied to the problem of Bayesian posterior sampling under a pretrained generative model prior  $p(x)$  by pulling the sampling problem back to its latent space.

Table 1: Comparison of data-to-data IPF methods. **Bold** indicates the best-performing method.

Distributions $\rightarrow$	Gauss $\leftrightarrow$ GMM		Gauss $\leftrightarrow$ Two Moons		Two Moons $\leftrightarrow$ GMM	
	$\mathcal{W}_2^2(\downarrow)$	Path KL ( $\downarrow$ )	$\mathcal{W}_2^2(\downarrow)$	Path KL ( $\downarrow$ )	$\mathcal{W}_2^2(\downarrow)$	Path KL ( $\downarrow$ )
DSBM-IMF (Shi et al., 2023)	0.046 $\pm$ 0.004	1.004 $\pm$ 0.137	0.061 $\pm$ 0.034	<b>1.813<math>\pm</math>0.960</b>	0.043 $\pm$ 0.012	<b>1.893<math>\pm</math>0.369</b>
DSBM-IMF+ (Shi et al., 2023)	0.060 $\pm$ 0.049	<b>0.909<math>\pm</math>0.426</b>	0.049 $\pm$ 0.007	1.848 $\pm$ 0.285	0.038 $\pm$ 0.010	<b>1.894<math>\pm</math>0.324</b>
[SF] <sup>2</sup> M (Tong et al., 2024b)	0.041 $\pm$ 0.021	2.295 $\pm$ 0.513	0.053 $\pm$ 0.022	3.321 $\pm$ 1.862	0.057 $\pm$ 0.030	3.823 $\pm$ 0.314
<i>IPF-based</i>						
DSB mean (De Bortoli et al., 2021)	0.093 $\pm$ 0.096	5.886 $\pm$ 4.460	0.111 $\pm$ 0.041	6.398 $\pm$ 1.949	0.078 $\pm$ 0.029	5.520 $\pm$ 3.163
DSB score (De Bortoli et al., 2021)	0.052 $\pm$ 0.018	5.645 $\pm$ 3.474	0.171 $\pm$ 0.149	14.346 $\pm$ 8.776	0.066 $\pm$ 0.035	5.231 $\pm$ 2.802
SDE (Chen et al., 2021b)	<b>0.037<math>\pm</math>0.010</b>	2.088 $\pm$ 1.228	0.033 $\pm$ 0.004	2.262 $\pm$ 0.268	<b>0.025<math>\pm</math>0.010</b>	3.915 $\pm$ 0.285
LL fixed var. $\approx$ Vargias et al. (2021)	<b>0.037<math>\pm</math>0.014</b>	2.507 $\pm$ 0.366	0.033 $\pm$ 0.005	2.351 $\pm$ 0.149	0.031 $\pm$ 0.011	3.710 $\pm$ 0.332
LL learnt var. (ours)	<b>0.042<math>\pm</math>0.018</b>	2.840 $\pm$ 0.668	<b>0.022<math>\pm</math>0.009</b>	4.288 $\pm$ 1.876	<b>0.023<math>\pm</math>0.013</b>	3.938 $\pm$ 0.526

Consider a posterior of the form  $p(x | y) \propto p(x)r(x, y)$ , where  $p(x)$  is a prior over the data space (*e.g.*, images) and  $r(x, y)$  is a constraint function that encodes the conditional information about the sample  $x$  (*e.g.*, a class likelihood or match to a text prompt). If the pretrained generative model is expressed as a deterministic function  $f$  of a random noise variable  $z \sim p(z)$ , Venkatraman et al. (2025) proposed to sample the posterior pulled back to the noise space, with density  $p(z | y) \propto p(z)r(f(z), y)$ , using a diffusion sampler. If  $z$  is distributed with this density, then samples  $f(z)$  follow the desired posterior distribution  $p(x | y)$  in data space. Such a method was successfully applied in the latent spaces of various models types, such as GANs, continuous normalising flows.

Instead of using a diffusion sampler, we propose to model a Schrödinger bridge between the distributions  $p(z)$  and  $p(z | y)$ . Since neither the normalising constant nor samples from the latter distribution are available, we use the data-to-energy algorithm described in §3.1. Modelling a Schrödinger bridge instead of simply a diffusion sampler has the advantage of transporting prior samples to nearby posterior samples in latent space, which is expected to preserve semantic content that is not constrained by  $y$ ; we show this empirically in §5.3.

**Metrics for outsourced stochastic transport.** In order to evaluate the performance of our method on the stochastic optimal transport task in the latent space, we compute path KL in the latent space, as well as the  $L^2$  static transport cost between prior samples from  $p_0(x_0)$  and the pushed-forward samples from the approximated posterior  $\vec{p}(\tau | x_0)p_0(x_0)$ . For image tasks with a classifier reward, in order to evaluate the quality of generated images with respect to the target posterior, we use the mean log-constraint value and FID (Heusel et al., 2017). The latter is computed between images decoded from latents sampled from the trained SB model and images of the target class(es), which are not available to the model during training.

## 5 EXPERIMENTS

### 5.1 BENEFITS OF TRAINABLE VARIANCE

In order to show the benefits of trainable variance in time-discretised processes, we present the comparisons of existing data-to-data SB methods with our proposed algorithms, including both learnt-variance and fixed-variance alternatives. The data-to-data experiments are conducted on several synthetic 2-dimensional benchmarks (following Shi et al. (2023)): Gauss  $\leftrightarrow$  GMM, Gauss  $\leftrightarrow$  Two Moons, Two Moons  $\leftrightarrow$  GMM (where Gauss is an isotropic Gaussian and GMM is a mixture of eight Gaussians). We compare with Shi et al. (2023) (DSBM and DSBM++), De Bortoli et al. (2021) (DSB), which also uses IPF for training, Chen et al. (2021b) (SDE), which uses a continuous-time version of IPF, and Tong et al. (2024b) ([SF]<sup>2</sup>M), which relies on a minibatch approximation to entropic optimal transport. All experiments use  $K = 20$  discretisation steps. The results in Table 1 clearly show the benefits of training the variances, despite the discrete-time processes not being consistent with an underlying continuous-time process.

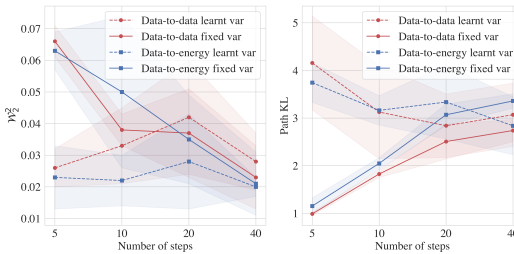


Figure 2:  $\mathcal{W}_2^2$  and Path KL depending on the number of discretization steps for Gauss  $\leftrightarrow$  GMM.

We further investigate the effect of learnt variance at varying numbers of discretisation steps. We find that learnt variance allows for more accurate modelling in both data-to-energy and data-to-data settings when the number of steps is small. Results are shown in Fig. 2 (in numerical form in Table 4).

For all 2-dimensional experiments we use  $dX_t = \sqrt{2} dW_t$  as the reference process; training is done using 4000 steps for both backward and forward processes and 20 IPF steps. We use the same neural network architecture for all 2-dimensional experiments. We provide a detailed experiment configuration in Appendix D.

## 5.2 DATA-TO-ENERGY AND ENERGY-TO-ENERGY SCHRÖDINGER BRIDGE

To prove the viability of data-to-energy Schrödinger bridge training we compare the bridge between Gaussian and GMM distributions trained using data-to-data and data-to-energy IPF versions (where the data-to-energy version has no access to the data samples that the data-to-data algorithm sees). Fig. 3 shows the resulting IPF trajectories and Table 4 shows that the data-to-energy model is comparable to one trained with data samples.

## 5.3 OUTSOURCED SCHRÖDINGER BRIDGE

Finally, we show the scalability of our method by running data-to-energy Schrödinger bridge algorithm in the latent space of generative model. We use the StyleGAN (Karras et al., 2020; 2021) and SN-GAN (Miyato et al., 2018) generators trained on CIFAR-10 (Krizhevsky, 2009), and VAE (Kingma & Welling, 2014; Rezende et al., 2014) generator trained on MNIST (LeCun et al., 1998). We train the bridge model between the latent space prior  $p(z)$ , which in our case is always a Gaussian distribution, and a reward-reweighted prior of the form  $r(f(z), y) \cdot p(z)$ . The reward function  $r(x, y)$  is a classifier that returns the probability of the object  $x$  belonging to the class  $y$  (i.e., the probability that  $x$  is, for example, a boat for CIFAR-10 or the digit 5 for MNIST).

MNIST experiments are conducted in two setups: (a) the reward function returns the probability that  $x$  is even or odd (b) the reward function returns the probability that  $x = 5$ . For CIFAR-10 experiments we use StyleGAN (Karras et al., 2020; 2021) generator with latent dimension 512 and SN-GAN (Miyato et al., 2018) generator with latent dimension 128. We use a pretrained classifier model as a reward function. Samples are shown in Fig. 4; more CIFAR-10 results can be found in Appendix F.

In Table 2 we compute FID between samples of the target class posterior obtained from the trained SB and images belonging to the target class in the dataset; we use the same metric for a set of ground truth posterior samples obtained by rejection sampling. Remarkably, the transported samples tend to have lower FID than samples from the true distribution.

These results reveal a benefit of training a Schrödinger bridge model, as opposed to a diffusion sampler or an arbitrary stochastic mapping. It can be seen in Fig. 4 that images already belonging to the target class change little, while those belonging to other classes maintain features that are unrelated to the target class: the background and global structure are preserved. This suggests that style transfer for higher-dimensional images can be a promising application of our method.

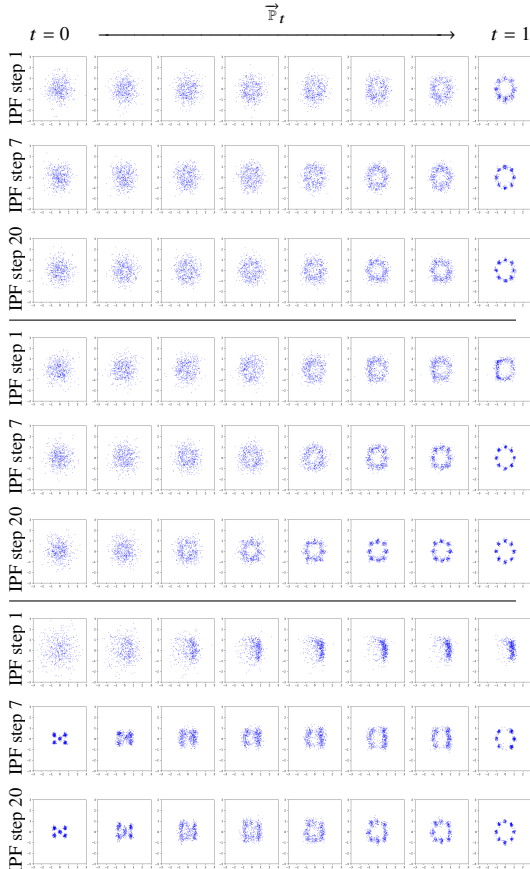


Figure 3: Comparison of learnt processes at various IPF iterations for data-to-data (*top*), data-to-energy (*middle*) and energy-to-energy (*bottom*) settings. For the energy-to-energy setting we use two different mixtures of Gaussian distributions.

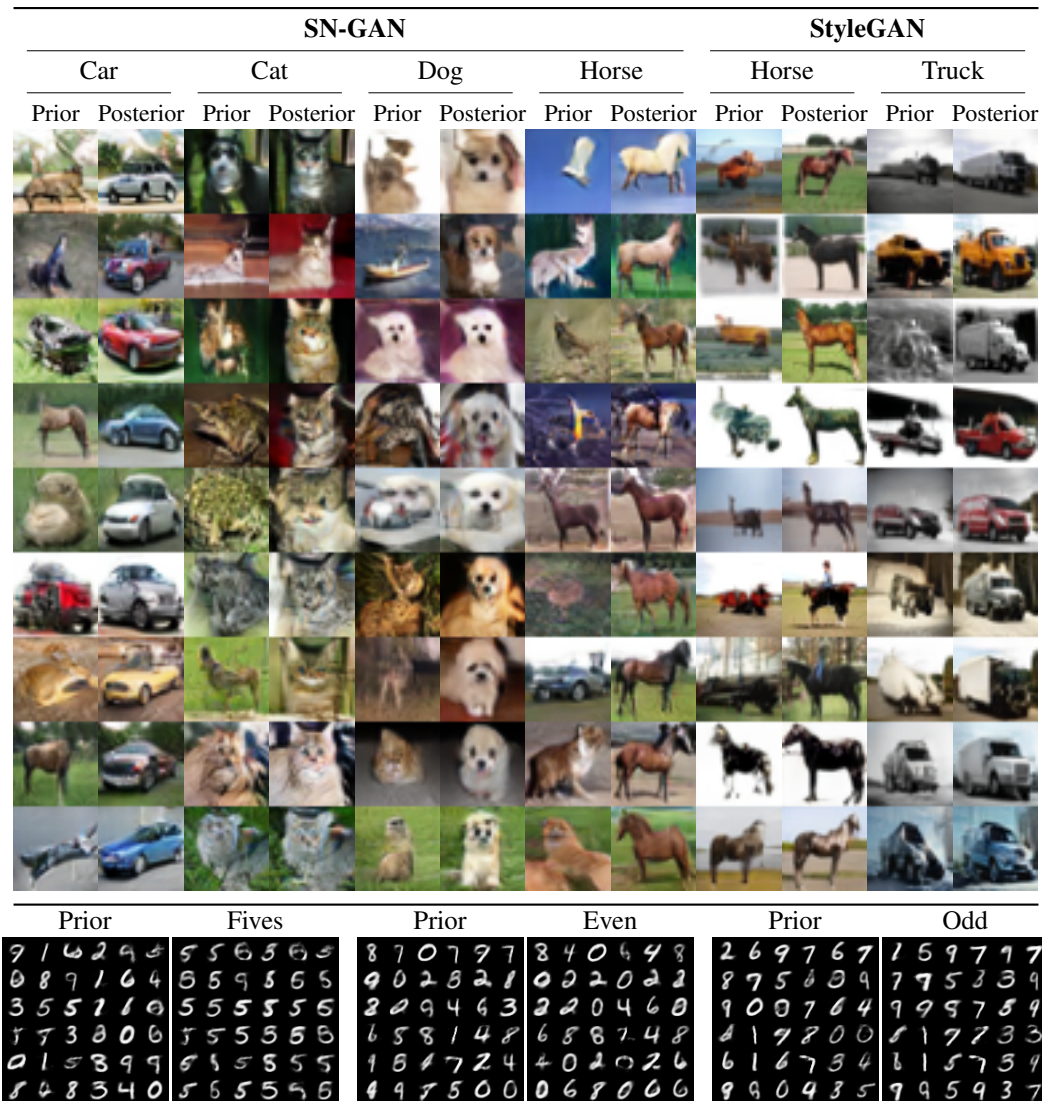


Figure 4: Outsourced Schrödinger bridge on MNIST and CIFAR-10. The bridge preserves style features (thickness, background colour, orientation) while transforming digits to the target class.

Table 2: ELBO ( $\uparrow$ ) values and FID ( $\downarrow$ ) scores comparing CIFAR-10 samples from the posterior under a GAN prior and a classifier to data samples of the target class. In this setting diffusion sampler performed worse than other methods, therefore, FID scores are computed only for ‘Dog’ and ‘Car’ classes.

Algorithm $\downarrow$ Class $\rightarrow$	SN-GAN				StyleGAN	
	Car	Cat	Dog	Horse	Horse	Truck
Same class	10.371	17.950	15.034	12.876	12.876	9.289
Rejection sampling	31.334	42.242	43.691	35.019	97.855	76.403
Langevin	25.296	33.619	37.665	27.601	85.611	68.678
Diffusion sampler	83.940	-	60.512	-	-	-
Outsourced SB	22.312	40.489	37.287	33.021	58.988	55.346
	ELBO					
Outsourced SB	-6.737	-9.356	-6.087	-5.961	-21.784	-6.809

Table 3: Ablation of off-policy reinforcement learning techniques on the SN-GAN outsourced sampling problem. **Bold** indicates the best result, underlined indicates second best. The model is trained to amortise sampling from one class (dogs).

Algorithm ↓ Metric →	ELBO (↑)	Path KL (↓)	$L_2^2(x_0, x_1)$ (↓)	mean log-reward (↑)
on-policy	-190.920	1506.407	10.949	-0.233
buffer	<u>-188.351</u>	622.895	10.957	<b>-0.125</b>
+ Langevin	-188.554	383.514	<u>10.130</u>	-0.286
+ reuse backward trajectory	<b>-188.149</b>	<b>206.094</b>	<b>10.046</b>	-0.657
+ annealed off-policy ratio	-188.355	<u>244.270</u>	11.386	-0.149
smaller off-policy ratio	-188.620	<u>668.255</u>	11.027	<u>-0.131</u>

#### 5.4 ABLATIONS OF OFF-POLICY TECHNIQUES

In order to verify our design choices for the high-dimensional experiments we provide a detailed ablation of the various off-policy reinforcement learning tricks described in §3.2. The results are given in Table 3. We use a simple on-policy setup as a baseline. We find that saving samples in a replay buffer (*buffer*) to use them for sampling backward trajectories and applying Langevin update to the buffer samples (*buffer + Langevin*) significantly improves the Path KL metrics, therefore yielding a bridge closer to the optimal one. Moreover, we show that reusing backward trajectories for the computation of loss also improves Path KL, giving the best model based on this metric. However, reusing backward trajectories negatively impacts the mean log-reward metric, possibly because it prevents mode collapse. To balance between modelling modes and achieving low transport cost, we explore the possibilities of both setting a smaller off-policy ratio – fraction of off-policy trajectories – and annealing the off-policy ratio throughout the training; the latter sometimes produces improvements. All ablation experiments are conducted using the SN-GAN generator and VGG13 classifier on the CIFAR-10 dataset. All models are trained to amortise sampling from one class (Dogs) and are trained with the same seed.

#### 5.5 COMPARISON WITH ANALYTICAL SOLUTION

To validate the proposed SB algorithm, we apply it to the problem of finding the SB between two Gaussians. In this case, the problem has an analytical solution (Bunne et al., 2023). For our experiments, we train SB between  $\mathcal{N}(0, I)$  and  $\mathcal{N}\left(\begin{bmatrix} 1 \\ 1 \end{bmatrix}, \begin{bmatrix} 3.0 & 1.2 \\ 1.2 & 1.0 \end{bmatrix}\right)$ . We compare the data-to-energy and data-to-data SB algorithms described in this paper, as well as DSBM (De Bortoli et al., 2021), to the SB computed analytically. For comparison, we use the Wasserstein-2 distance computed between samples obtained from the SB algorithm and analytical solution, for each time step of the trajectory. The results are in Fig. 5.

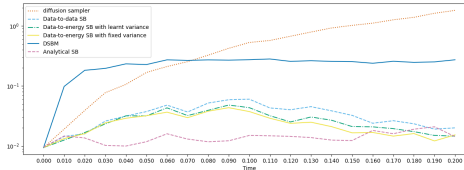


Figure 5: SB algorithms’ comparison in  $\mathcal{W}_2$  to the analytical solution.

## 6 CONCLUSION

This paper shows the potential of training data-to-energy Schrödinger bridges in a time discretisation with learnable drift and variance for the forward and backward processes. We showed that, despite its complexity, our method can be successfully scaled. Future work should focus more on scaling the data-to-energy Schrödinger bridges to higher dimensions, as well as arbitrary prior distributions, which would significantly improve the versatility of the proposed algorithms. Moreover, the trained samplers are prone to mode collapse, therefore, future work should investigate techniques to further improve mode coverage. One more promising direction would be to amortise over the distribution of conditions in image generation problems, instead of learning a model for each specific condition. Finally, we are excited to explore various domains in which the proposed algorithms can be applied. Interesting areas include text-conditional image reward fine-tuning of diffusion models and discrete Schrödinger bridge problems (recently explored in Carter et al. (2026)).

## ACKNOWLEDGEMENTS

The authors thank Sanghyeok Choi for comments on the manuscript.

This work was enabled by the computational resources of the Edinburgh International Data Facility (EIDF) with funding from the Edinburgh Generative AI Laboratory (GAIL).

NM acknowledges support from the CIFAR Learning in Machines and Brains programme.

## REFERENCES

- Michael S Albergo, Nicholas M Boffi, and Eric Vanden-Eijnden. Stochastic interpolants: A unifying framework for flows and diffusions. *Journal of Machine Learning Research*, 26(209):1–80, 2025.
- Michael Samuel Albergo and Eric Vanden-Eijnden. NETS: A non-equilibrium transport sampler. *International Conference on Machine Learning (ICML)*, 2025.
- Arip Asadulaev, Rostislav Korst, Vitalii Shutov, Alexander Korotin, Yaroslav Grebnyak, Vahe Egiazarian, and Evgeny Burnaev. Optimal transport maps are good voice converters. *arXiv preprint arXiv:2411.02402*, 2024.
- Jimmy Lei Ba, Jamie Ryan Kiros, and Geoffrey E Hinton. Layer normalization. *arXiv preprint arXiv:1607.06450*, 2016.
- Julius Berner, Lorenz Richter, and Karen Ullrich. An optimal control perspective on diffusion-based generative modeling. *Transactions on Machine Learning Research*, 2024.
- Julius Berner, Lorenz Richter, Marcin Sendera, Jarrid Rector-Brooks, and Nikolay Malkin. From discrete-time policies to continuous-time diffusion samplers: Asymptotic equivalences and faster training. *Transactions on Machine Learning Research (TMLR)*, 2026.
- Denis Blessing, Julius Berner, Lorenz Richter, and Gerhard Neumann. Underdamped diffusion bridges with applications to sampling. *International Conference on Learning Representations (ICLR)*, 2025a.
- Denis Blessing, Xiaogang Jia, and Gerhard Neumann. End-to-end learning of Gaussian mixture priors for diffusion sampler. *International Conference on Learning Representations (ICLR)*, 2025b.
- Charlotte Bunne, Ya-Ping Hsieh, Marco Cuturi, and Andreas Krause. The schrödinger bridge between gaussian measures has a closed form. *International Conference on Artificial Intelligence and Statistics (AISTATS)*, 2023.
- Arran Carter, Sanghyeok Choi, Kirill Tamogashev, Víctor Elvira, and Nikolay Malkin. Discrete diffusion samplers and bridges: Off-policy algorithms and applications in latent spaces. *arXiv preprint arXiv:2602.05961*, 2026.
- Nanxin Chen, Yu Zhang, Heiga Zen, Ron J Weiss, Mohammad Norouzi, and William Chan. Wave-Grad: Estimating gradients for waveform generation. *International Conference on Learning Representations (ICLR)*, 2021a.
- Tianrong Chen, Guan-Hong Liu, and Evangelos Theodorou. Likelihood training of Schrödinger bridge using forward-backward SDEs theory. *International Conference on Learning Representations (ICLR)*, 2021b.
- Yongxin Chen, Tryphon T Georgiou, and Michele Pavon. Optimal transport in systems and control. *Annual Review of Control, Robotics, and Autonomous Systems*, 4(1):89–113, 2021c.
- Valentin De Bortoli, James Thornton, Jeremy Heng, and Arnaud Doucet. Diffusion Schrödinger bridge with applications to score-based generative modeling. *Neural Information Processing Systems (NeurIPS)*, 2021.
- W Edwards Deming and Frederick F Stephan. On a least squares adjustment of a sampled frequency table when the expected marginal totals are known. *The Annals of Mathematical Statistics*, 11(4): 427–444, 1940.

- Prafulla Dhariwal and Alexander Nichol. Diffusion models beat GANs on image synthesis. *Neural Information Processing Systems (NeurIPS)*, 2021.
- Robert Fortet. Résolution d’un système d’équations de M. Schrödinger. *Journal de mathématiques pures et appliquées*, 19(1-4):83–105, 1940.
- Milena Gazdieva, Petr Mokrov, Litu Rout, Alexander Korotin, Andrey Kravchenko, Alexander Filipov, and Evgeny Burnaev. An optimal transport perspective on unpaired image super-resolution. *Journal of Optimization Theory and Applications*, 207(2):40, 2025.
- Timofei Gritsaev, Nikita Morozov, Kirill Tamogashev, Daniil Tiapkin, Sergey Samsonov, Alexey Naumov, Dmitry Vetrov, and Nikolay Malkin. Adaptive destruction processes for diffusion samplers. *arXiv preprint arXiv:2506.01541*, 2025.
- Martin Heusel, Hubert Ramsauer, Thomas Unterthiner, Bernhard Nessler, and Sepp Hochreiter. GANs trained by a two time-scale update rule converge to a local nash equilibrium. *Neural Information Processing Systems (NeurIPS)*, 2017.
- Jonathan Ho, Ajay Jain, and Pieter Abbeel. Denoising diffusion probabilistic models. *Neural Information Processing Systems (NeurIPS)*, 2020.
- Jian Huang, Yuling Jiao, Lican Kang, Xu Liao, Jin Liu, and Yanyan Liu. Schrödinger–Föllmer sampler. *IEEE Transactions on Information Theory*, 71:1283–1299, 2021.
- Leonid V. Kantorovich. Mathematical methods of organizing and planning production. *Management science*, 6(4):366–422, 1960.
- Leonid V. Kantorovich and Gennady S. Rubinshtein. On a space of totally additive functions. *Vestnik of the St. Petersburg University: Mathematics*, 13(7):52–59, 1958.
- Tero Karras, Samuli Laine, Miika Aittala, Janne Hellsten, Jaakko Lehtinen, and Timo Aila. Analyzing and improving the image quality of stylegan. *Computer Vision and Pattern Recognition (CVPR)*, 2020.
- Tero Karras, Miika Aittala, Samuli Laine, Erik Härkönen, Janne Hellsten, Jaakko Lehtinen, and Timo Aila. Alias-free generative adversarial networks. *Neural Information Processing Systems (NeurIPS)*, 2021.
- Diederik P Kingma and Max Welling. Auto-encoding variational bayes. *International Conference on Learning Representations (ICLR)*, 2014.
- Zhifeng Kong, Wei Ping, Jiaji Huang, Kexin Zhao, and Bryan Catanzaro. DiffWave: A versatile diffusion model for audio synthesis. *International Conference on Learning Representations (ICLR)*, 2021.
- Alexander Korotin, Daniil Selikhanovych, and Evgeny Burnaev. Neural optimal transport. *International Conference on Learning Representations (ICLR)*, 2022.
- Alex Krizhevsky. Learning multiple layers of features from tiny images. Technical Report TR-2009, University of Toronto, 2009.
- Salem Lahlou, Tristan Deleu, Pablo Lemos, Dinghuai Zhang, Alexandra Volokhova, Alex Hernández-García, Léna Néhale Ezzine, Yoshua Bengio, and Nikolay Malkin. A theory of continuous generative flow networks. *International Conference on Machine Learning (ICML)*, 2023.
- Yann LeCun, Léon Bottou, Yoshua Bengio, and Patrick Haffner. Gradient-based learning applied to document recognition. *Proceedings of the IEEE*, 86(11):2278–2324, 1998.
- Yaron Lipman, Ricky TQ Chen, Heli Ben-Hamu, Maximilian Nickel, and Matt Le. Flow matching for generative modeling. *International Conference on Learning Representations (ICLR)*, 2023.
- Xingchao Liu, Chengyue Gong, and Qiang Liu. Flow straight and fast: Learning to generate and transfer data with rectified flow. *International Conference on Learning Representations (ICLR)*, 2023.

- Christian Léonard. A survey of the Schrödinger problem and some of its connections with optimal transport. *Discrete and Continuous Dynamical Systems*, 34(4):1533–1574, 2014.
- Nikolay Malkin, Moksh Jain, Emmanuel Bengio, Chen Sun, and Yoshua Bengio. Trajectory balance: Improved credit assignment in GFlowNets. *Neural Information Processing Systems (NeurIPS)*, 2022.
- Takeru Miyato, Toshiki Kataoka, Masanori Koyama, and Yuichi Yoshida. Spectral normalization for generative adversarial networks. *International Conference on Learning Representations (ICLR)*, 2018.
- Gaspard Monge. *Mémoire sur la Théorie des Déblais et des Remblais*. Imprimerie royale, 1781.
- Shen Nie, Fengqi Zhu, Zebin You, Xiaolu Zhang, Jingyang Ou, Jun Hu, Jun Zhou, Yankai Lin, Ji-Rong Wen, and Chongxuan Li. Large language diffusion models. *Neural Information Processing Systems (NeurIPS)*, 2025.
- Gabriel Peyré, Marco Cuturi, et al. Computational optimal transport: With applications to data science. *Foundations and Trends in Machine Learning*, 11(5-6):355–607, 2019.
- Adam Polyak, Amit Zohar, Andrew Brown, Andros Tjandra, Animesh Sinha, Ann Lee, Apoorv Vyas, Bowen Shi, Chih-Yao Ma, Ching-Yao Chuang, et al. Movie Gen: A cast of media foundation models. *arXiv preprint arXiv:2410.13720*, 2024.
- Danilo Jimenez Rezende, Shakir Mohamed, and Daan Wierstra. Stochastic backpropagation and approximate inference in deep generative models. *International Conference on Machine Learning (ICML)*, 2014.
- Lorenz Richter and Julius Berner. Improved sampling via learned diffusions. *International Conference on Learning Representations (ICLR)*, 2024.
- Lorenz Richter, Ayman Boustati, Nikolas Nüsken, Francisco Ruiz, and Omer Deniz Akyildiz. Var-Grad: a low-variance gradient estimator for variational inference. *Neural Information Processing Systems (NeurIPS)*, 2020.
- Robin Rombach, A. Blattmann, Dominik Lorenz, Patrick Esser, and Björn Ommer. High-resolution image synthesis with latent diffusion models. *Computer Vision and Pattern Recognition (CVPR)*, 2021.
- Subham Sekhar Sahoo, Justin Deschenaux, Aaron Gokaslan, Guanghan Wang, Justin T Chiu, and Volodymyr Kuleshov. The diffusion duality. *International Conference on Machine Learning (ICML)*, 2025.
- Erwin Schrödinger. Über die umkehrung der naturgesetze. *Sitzungsberichte der Preussischen Akademie der Wissenschaften, Physikalisch-mathematische Klasse*, pp. 144–153, 1931.
- Erwin Schrödinger. Sur la théorie relativiste de l’électron et l’interprétation de la mécanique quantique. *Annales de l’Institut Henri Poincaré*, 2(4):269–310, 1932.
- Marcin Sendera, Minsu Kim, Sarthak Mittal, Pablo Lemos, Luca Scimeca, Jarrid Rector-Brooks, Alexandre Adam, Yoshua Bengio, and Nikolay Malkin. Improved off-policy training of diffusion samplers. *Neural Information Processing Systems (NeurIPS)*, 2024.
- Yuyang Shi, Valentin De Bortoli, Andrew Campbell, and Arnaud Doucet. Diffusion Schrödinger bridge matching. *Neural Information Processing Systems (NeurIPS)*, 2023.
- Karen Simonyan and Andrew Zisserman. Very deep convolutional networks for large-scale image recognition. *International Conference on Learning Representations (ICLR)*, 2015.
- Richard Sinkhorn. A relationship between arbitrary positive matrices and doubly stochastic matrices. *The annals of mathematical statistics*, 35(2):876–879, 1964.
- Jascha Sohl-Dickstein, Eric A. Weiss, Niru Maheswaranathan, and Surya Ganguli. Deep unsupervised learning using nonequilibrium thermodynamics. *International Conference on Machine Learning (ICML)*, 2015.

- Yang Song, Conor Durkan, Iain Murray, and Stefano Ermon. Maximum likelihood training of score-based diffusion models. *Neural Information Processing Systems (NeurIPS)*, 2021a.
- Yang Song, Jascha Sohl-Dickstein, Diederik P Kingma, Abhishek Kumar, Stefano Ermon, and Ben Poole. Score-based generative modeling through stochastic differential equations. *International Conference on Learning Representations (ICLR)*, 2021b.
- Austin Stromme. Sampling from a Schrödinger bridge. *Artificial Intelligence and Statistics (AISTATS)*, 2023.
- Simo Särkkä and Arno Solin. *Applied stochastic differential equations*, volume 10. Cambridge University Press, 2019.
- Alexander Tong, Kilian FATRAS, Nikolay Malkin, Guillaume Hugué, Yanlei Zhang, Jarrid Rector-Brooks, Guy Wolf, and Yoshua Bengio. Improving and generalizing flow-based generative models with minibatch optimal transport. *Transactions on Machine Learning Research*, 2024a.
- Alexander Tong, Nikolay Malkin, Kilian Fatras, Lazar Atanackovic, Yanlei Zhang, Guillaume Hugué, Guy Wolf, and Yoshua Bengio. Simulation-free Schrödinger bridges via score and flow matching. *Artificial Intelligence and Statistics (AISTATS)*, 2024b.
- Belinda Tzen and Maxim Raginsky. Neural stochastic differential equations: Deep latent Gaussian models in the diffusion limit. *arXiv preprint arXiv:1905.09883*, 2019.
- Francisco Vargas, Pierre Thodoroff, Austen Lamacraft, and Neil Lawrence. Solving Schrödinger bridges via maximum likelihood. *Entropy*, 23(9):1134, August 2021.
- Francisco Vargas, Will Grathwohl, and Arnaud Doucet. Denoising diffusion samplers. *International Conference on Learning Representations (ICLR)*, 2023.
- Francisco Vargas, Shreyas Padhy, Denis Blessing, and Nikolas Nüsken. Transport meets variational inference: Controlled monte carlo diffusions. *International Conference on Learning Representations (ICLR)*, 2024.
- Siddarth Venkatraman, Mohsin Hasan, Minsu Kim, Luca Scimeca, Marcin Sendera, Yoshua Bengio, Glen Berseth, and Nikolay Malkin. Outsourced diffusion sampling: Efficient posterior inference in latent spaces of generative models. *International Conference on Machine Learning (ICML)*, 2025.
- Cédric Villani. *Optimal transport: old and new*, volume 338. Springer, 2008.
- Qinsheng Zhang and Yongxin Chen. Path Integral Sampler: A stochastic control approach for sampling. *International Conference on Learning Representations (ICLR)*, 2022.

## A RELATED WORKS

In this section we establish links between our method and other research directions in the literature.

**Optimal transport.** Optimal transport is a well-established area of research with a solid theoretical background and scalable applied algorithms. The problem is concerned with finding the optimal transportation map which minimises a given transportation cost. Originally, the problem was proposed by Monge (Monge, 1781). In 20th century this problem was reformulated and generalised by Kantorovich in a series of works including Kantorovich & Rubinshtein (1958); Kantorovich (1960). Since then the problem has been rigorously studied, refer to Peyré et al. (2019); Villani (2008) for a detailed presentation of theory. In a discrete case optimal transport can be solved using Sinkhorn’s algorithm (Sinkhorn, 1964; Peyré et al., 2019). Recent works have applied optimal transport to a series of machine learning problems, including image-to-image translation (Korotin et al., 2022), voice conversion (Asadulaev et al., 2024), and super-resolution (Gazdieva et al., 2025).

**Schrödinger bridges.** The Schrödinger bridge problem is concerned with finding stochastic optimal transport dynamics between two distributions. The problem was originally proposed by Schrödinger (Schrödinger, 1931; 1932). The Schrödinger bridge problem can be seen as a regularised version of dynamic optimal transport (Léonard, 2014) and has interesting connections to optimal control theory (Chen et al., 2021c). Computationally, the problem can be solved using Iterative Proportional Fitting (IPF) algorithm (Fortet, 1940; Deming & Stephan, 1940; Sinkhorn, 1964). De Bortoli et al. (2021); Vargas et al. (2021) proposed the scalable formulation of this method that allows to compute Schrödinger bridge between a pair of distributions given by unbiased samples. Chen et al. (2021b) proposes a continuous-time variant of IPF. Methods distinct from IPF have also been proposed (Shi et al., 2023; Tong et al., 2024b); all of them assume access to samples from the target distribution for an unbiased objective.

**Diffusion samplers.** Data-to-energy Schrödinger bridge is related to the problem of sampling from an unnormalised density. Diffusion samplers (Zhang & Chen, 2022; Vargas et al., 2023; Richter & Berner, 2024; Berner et al., 2024; Blessing et al., 2025a) represent one of the approaches that solve this problem. Some methods use off-policy reinforcement learning techniques (Lahlou et al., 2023; Sendera et al., 2024) to amortise sampling from intractable density. The theoretical connection among various objectives was established in Berner et al. (2026).

**Outsourced sampling.** The concept of outsourced diffusion sampling – modelling continuous-time dynamics in latent space for posterior inference under pretrained priors – was proposed in Venkatraman et al. (2025). The work shows that sampling can be efficiently conducted in the latent space of a generator, where the density landscape is smoother.

## B METRICS FOR DATA-TO-ENERGY SB

First, if both samples from  $p_0$  and the density of  $p_0$  are available, we evaluate the quality of the learnt  $\vec{p}_\theta$  as a sampler of  $p_1$  using the evidence lower bound:

$$\text{ELBO} = \mathbb{E}_{x_0 \sim p_0(x_0), \tau \sim \vec{p}_\theta(\tau | x_0)} \left[ \log \frac{\overleftarrow{p}_\varphi(\tau | x_1) \exp(-\mathcal{E}_1(x_1))}{\vec{p}_\theta(\tau | x_0) p_0(x_0)} \right] \leq \log Z,$$

which equals the true  $\log Z = \log \int \exp(-\mathcal{E}_1(x)) dx$  if and only if the processes  $\vec{p}_\theta$  and  $\overleftarrow{p}_\varphi$  coincide.

Second, if samples from  $p_1$  are available (even if not available to the learner during training), we report the 2-Wasserstein distance  $\mathcal{W}_2$  between batches of true samples from  $p_1(x_1)$  and samples obtained from the learnt model  $p_\theta(\tau | x_0)$ , which measures the discrepancy between the target and modelled marginals.

Third, to approximate the cost, we compute the path KL in discrete time:

$$\text{KL}(p_0 \otimes \vec{\mathbb{P}}_{t|0} \| p_0 \otimes \mathbb{Q}_{t|0}) \approx \text{KL}\left(p_0(x_0) \otimes \vec{p}_\theta(\tau | x_0) \| p_0(x_0) \otimes q(\tau | x_0)\right) \quad (9)$$

$$= \mathbb{E}_{x_0 \sim p_0, \tau \sim \vec{p}_\theta(\tau | x_0)} \left[ \log \frac{\vec{p}_\theta(\tau | x_0)}{q(\tau | x_0)} \right] \quad (10)$$

$$= \mathbb{E}_{x_0 \sim p_0, \tau \sim \vec{p}_\theta(\tau | x_0)} \left[ \sum_{k=0}^{K-1} \text{KL}(\vec{p}_\theta(x'_{k+1} | x_k) \| q(x'_{k+1} | x_k)) \right] \quad (11)$$

where  $q(\tau)$  is the time discretisation of the reference process  $\mathbb{Q}_t$ . The estimator using transition KLs in (11) can be seen to be a Rao-Blackwellised (lower-variance) variant of the estimator in (10), and we use it because the KL can be computed analytically (as all transition kernels are Gaussian). It can be shown (Appendix C) that this path KL is equivalent to path energy as used in Shi et al. (2023).

## C RELATION BETWEEN PATH KL AND PATH ENERGY

In this section we explain the relation between path KL and path energy (Shi et al., 2023). Assuming that the transition kernels are given by:

$$\vec{p}_\theta(x'_{k+1} | x_k) = \mathcal{N}\left(x_k + v_\theta(x_k, k\Delta t)\Delta t, \sigma^2\Delta t I\right) \quad (12)$$

$$q(x'_{k+1} | x_k) = \mathcal{N}\left(x_k, \sigma^2\Delta t I\right) \quad (13)$$

where  $v_\theta(x_t, t)$  is a learnt drift,  $\sigma^2$  is constant and is the same for both  $\mathbb{P}_{t|0}$  and  $\mathbb{Q}_{t|0}$ , time-discrete path KL can be written in the following form:

$$\text{KL}\left(p_0(x_0) \otimes \vec{p}_\theta(\tau | x_0) \| p_0(x_0) \otimes q(\tau | x_0)\right) \quad (14)$$

$$= \mathbb{E}_{x_0 \sim p_0, \tau \sim \vec{p}_\theta(\tau | x_0)} \left[ \log \frac{\vec{p}_\theta(\tau | x_0)}{q(\tau | x_0)} \right] = \mathbb{E}_{x_0 \sim p_0, \tau \sim \vec{p}_\theta(\tau | x_0)} \left[ \sum_{k=0}^{K-1} \log \frac{\vec{p}_\theta(x'_{k+1} | x_k)}{q(x'_{k+1} | x_k)} \right] \quad (15)$$

$$= \mathbb{E}_{x_0 \sim p_0, \tau \sim \vec{p}_\theta(\tau | x_0)} \left[ \sum_{k=0}^{K-1} \left( \frac{v_\theta(x_k, k\Delta t)}{\sigma^2} (x_{k+1} - x_k) - \frac{\|v_\theta(x_k, k\Delta t)\|^2}{2\sigma^2} \Delta t \right) \right] \quad (16)$$

Given that  $x_{k+1} - x_k = v_\theta(x'_k, k\Delta t)\Delta t + \sigma\sqrt{\Delta t}\xi_k$ ,  $\xi_k \sim \mathcal{N}(0, I)$  for  $0 \leq k \leq K-1$  and the  $\xi_{k_i}$  are independent, the path KL can be finally written as:

$$\text{KL}\left(p_0(x_0) \otimes \vec{p}_\theta(\tau | x_0) \| p_0(x_0) \otimes q(\tau | x_0)\right) \quad (17)$$

$$= \mathbb{E}_{x_0 \sim p_0, \tau \sim \vec{p}_\theta(\tau | x_0)} \left[ \sum_{k=0}^{K-1} \frac{\|v_\theta(x_k, k\Delta t)\|^2}{2\sigma^2} \Delta t \right] \xrightarrow{\Delta t \rightarrow 0} \frac{1}{2\sigma^2} \mathbb{E}_{p_0(x_0) \otimes \vec{p}_\theta(\tau | x_0)} \left[ \int \|v_\theta(x_t, t)\|^2 dt \right] \quad (18)$$

The limit is justified by the Girsanov theorem (Särkkä & Solin, 2019). This yields the path energy used in Shi et al. (2023).

## D EXPERIMENT DETAILS

### D.1 DATA-TO-DATA EXPERIMENTS

All data-to-data experiments are conducted under the unified setup. For the neural network we use an MLP with 3 hidden layers and 64 neurons in each layer; each layer is followed by a LayerNorm (Ba et al., 2016) and SiLU activation function. All neural networks are trained using AdamW optimiser with learning rate 0.0008. Sampling is done in 20 steps with  $t_{\max} = 0.2$  and  $dt = 0.01$ . We train forward and backward models for 4000 steps at each IPF iteration and we train each model for 20 IPF iterations. [SF]<sup>2</sup>M is trained using 160,000 steps. The metrics are computed using 10,000 samples from the target distributions and 10,000 samples obtained from the learnt forward process. All the metrics are averaged over 5 seeds (42, 43, 44, 45, 46).

## D.2 2D DATA-TO-ENERGY EXPERIMENTS

For the data-to-energy experiments we use the same neural networks as for data-to-data experiments. We use 20 steps for sampling with  $t_{\max} = 0.8$  and  $dt = 0.04$ . Neural networks are optimised with AdamW optimiser with learning rate 0.0005. When Langevin update is used, we update buffer samples every 500 steps during training of the forward process. Langevin is used with the step size 0.01 and we do 50 updates each time. We use 2 trajectories from each  $x_0$  for the computation of the VarGrad loss. All the metrics are averaged over 5 seeds (42, 43, 44, 45, 46).

## D.3 2D ENERGY-TO-ENERGY EXPERIMENTS

We provide a description of energy-to-energy experiment shown in Fig. 3. We use GMM with 5 modes for the distribution  $p_0$  and GMM with 8 modes for distribution  $p_1$ . For both distributions we rely exclusively on the corresponding log-densities. We do not use samples from either  $p_0$  or  $p_1$ . We keep replay buffers for both densities. We initialise both replay buffers with Gaussian noise at the beginning of training. Since samples are unavailable, we use the objective Equation (7) to learn the forward process and a similar objective:

$$\mathcal{L}_{LV}(x_1, \varphi) = \text{Var} \left( \log \frac{\overleftarrow{p}_\varphi(\tau | x_1)}{\overrightarrow{p}_\theta(\tau | x_0)p_0(x_0)} \right) = \text{Var} \left( \sum_{k=1}^K \log \frac{\overleftarrow{p}_\varphi(x_{(k-1)\Delta t} | x_{k\Delta t})}{\overrightarrow{p}_\theta(x_{k\Delta t} | x_{(k-1)\Delta t})} + \mathcal{E}_0(x_0) \right), \quad (19)$$

to learn the backward process.

## D.4 OUTSOURCED SCHRÖDINGER BRIDGE EXPERIMENTS

**Experiments on MNIST.** For MNIST experiments, we use a custom VAE with 3 layers in both the decoder and encoder. We use a custom MNIST classifier as a reward model, which consists of 3 MLP layers. Each layer is followed by the ReLU activation function, except for the last one, which uses a sigmoid. We train the forward and backward networks for 5,000 steps during each IPF iteration, with 20 IPF iterations in total. All the networks are trained with AdamW optimiser using learning rate 0.0008. We do not use Langevin updates for this experiment, relying only on a replay buffer. We use the same MLPs as in 2D data-to-energy experiment to parameterise the backward and forward drift and variance.

**Experiments on CIFAR-10 with SN-GAN and StyleGAN.** For the CIFAR-10 experiments, we use MLP with 3 hidden layers, which has 256 hidden units for the SN-GAN experiments and 512 for the StyleGAN experiments. We train forward network for 500 steps and backward network for 100 steps during each IPF iteration, for a total of 300 IPF iterations. All the networks are trained with AdamW optimiser using learning rate 0.0005. Langevin updates are made every 500 iterations during the training of the forward network. We run Langevin for 500 steps with initial step size of 0.01 and anneal step size to 0.001 during the updates.

We use 20 steps for sampling with  $dt = 0.04$  for the StyleGAN experiments and  $dt = 0.005$  for SN-GAN experiments. We use Wiener process,  $dX_t = \sqrt{2}dW_t$ , as the reference process. All the main experiments are conducted with a replay buffer and Langevin updates, with off-policy ratio of 0.8, and the backward trajectories are reused for computing VarGrad loss.

For the reward model we use VGG (Simonyan & Zisserman, 2015) classifier pretrained on CIFAR-10. The weights are taken from [https://github.com/huyvnphan/PyTorch\\_CIFAR10](https://github.com/huyvnphan/PyTorch_CIFAR10). We use VGG-13 for SN-GAN experiments and VGG-19 for StyleGAN experiments.

For the rejection sampling (ground truth), the FID score is computed between 6,000 images sampled proportional to the probabilities obtained from classifier and 6,000 images from the CIFAR-10 dataset. For the outsourced SB the FID score is computed between 6,000 samples from the learnt model and 6,000 real CIFAR-10 samples. All scores are computed only on the images of a specific class. All other metrics (path KL, mean log-reward,  $L_2^2(x_0, x_1)$ , ELBO) are computed using a batch size of 512.

Table 4: SB metrics for varying the number of time discretisation steps in data-to-data and data-to-energy setting with both learnt and fixed variance (Gauss  $\leftrightarrow$  GMM).

Number of steps $\rightarrow$	$K = 5$		$K = 10$		$K = 20$		$K = 40$	
	$\mathcal{W}_2^2$	Path KL	$\mathcal{W}_2^2$	Path KL	$\mathcal{W}_2^2$	Path KL	$\mathcal{W}_2^2$	Path KL
Data-to-data learnt var.	0.026 $\pm$ 0.006	4.158 $\pm$ 0.986	0.033 $\pm$ 0.012	3.127 $\pm$ 0.981	0.042 $\pm$ 0.018	2.840 $\pm$ 0.668	0.028 $\pm$ 0.009	3.070 $\pm$ 0.666
Data-to-data fixed var.	0.066 $\pm$ 0.005	0.988 $\pm$ 0.031	0.038 $\pm$ 0.005	1.825 $\pm$ 0.073	0.037 $\pm$ 0.014	2.507 $\pm$ 0.366	0.023 $\pm$ 0.010	2.739 $\pm$ 0.233
Data-to-energy learnt var	0.023 $\pm$ 0.010	3.745 $\pm$ 0.415	0.022 $\pm$ 0.008	3.162 $\pm$ 0.308	0.028 $\pm$ 0.015	3.337 $\pm$ 0.775	0.020 $\pm$ 0.003	2.838 $\pm$ 0.609
Data-to-energy fixed var	0.063 $\pm$ 0.006	1.152 $\pm$ 0.172	0.050 $\pm$ 0.024	2.047 $\pm$ 0.123	0.035 $\pm$ 0.014	3.069 $\pm$ 0.226	0.021 $\pm$ 0.010	3.360 $\pm$ 0.150

## E ADDITIONAL RESULTS

In addition to Fig. 2 we also provide the metrics for the ablation in Table 4. We use the same architecture and hyperparameters as in data-to-data experiments and vary only the number of sampling steps. For the data-to-energy runs we use a replay buffer with Langevin updates, the off-policy ratio is set to 0.8 and the backward trajectories are not reused for the loss computation.  $\mathcal{W}_2^2$  is computed using 10,000 ground truth samples and samples from  $\vec{p}(\tau | x_0)p_0(x_0)$ . Path KL is also computed on 10,000 samples.

## F VISUAL EXAMPLES FOR OUTSOURCED SB

### F.1 UNCURATED EXAMPLES



Figure 6: Uncurated examples of outsourced SB with SN-GAN for the class cars.



Figure 7: Uncurated examples of outsourced SB with SN-GAN for the class *cats*.

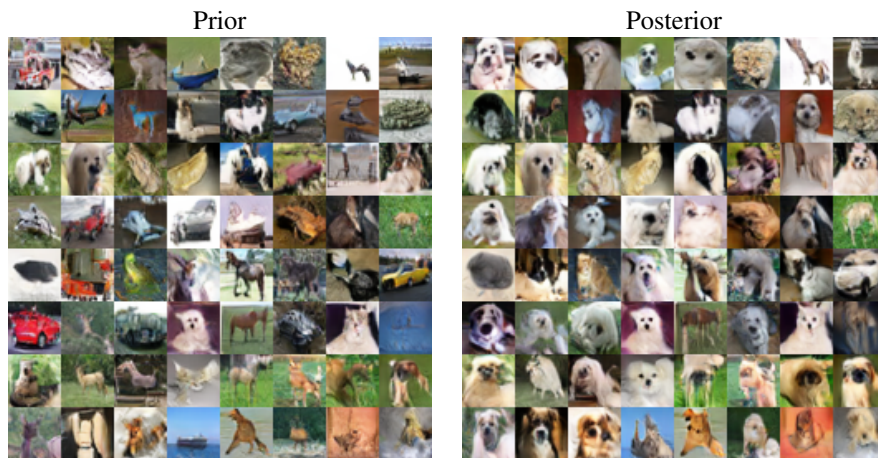


Figure 8: Uncurated examples of outsourced SB with SN-GAN for the class *dogs*.

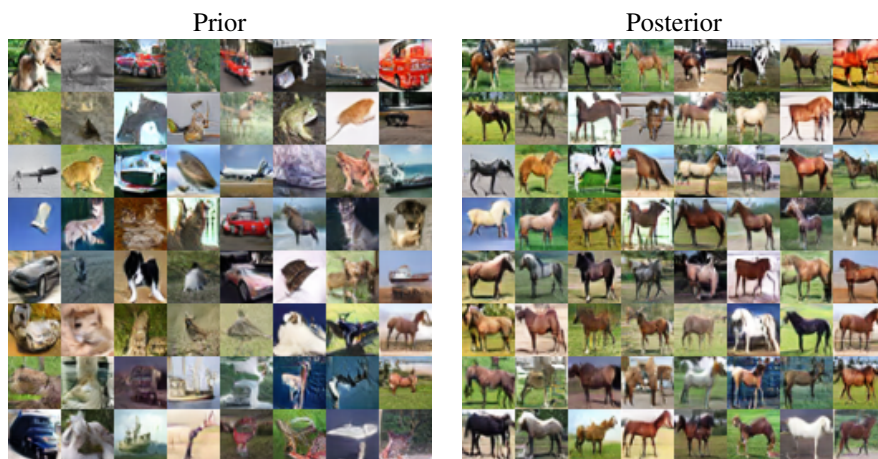


Figure 9: Uncurated examples of outsourced SB with SN-GAN for the class *horses*.



Figure 10: Uncurated examples of outsourced SB with StyleGAN for the class *horses*.



Figure 11: Uncurated examples of outsourced SB with StyleGAN for the class *trucks*.

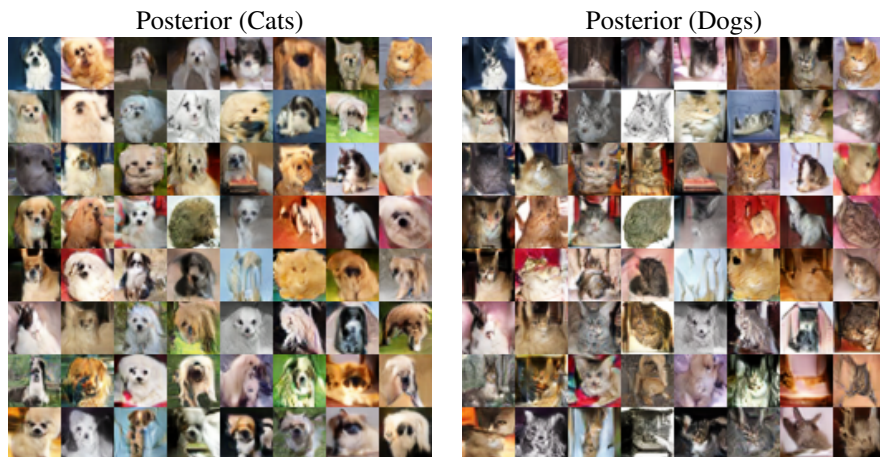


Figure 12: Uncurated examples of outsourced SB with SN-GAN between classes *cats* and *dogs*.

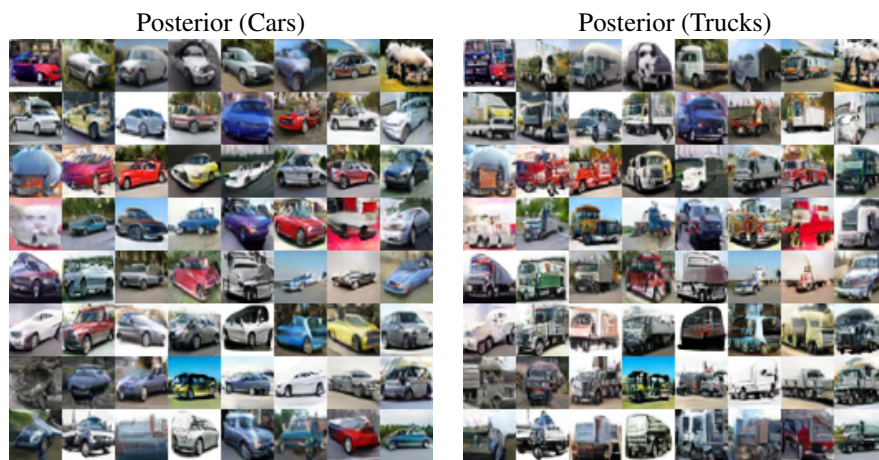


Figure 13: Uncurated examples of outsourced SB with SN-GAN between classes *cars* and *trucks*.